JOURNAL OF COMPUTATIONAL PHYSICS **142,** 67–79 (1998)
ARTICLE NO. CP985932

A Time-Domain Method for the Determination of Unsteady Pressure with a Tube of Constant Cross-Section

K. Ehrendorfer, F. Ottitsch, and H. Sockel

Institut für Strömungslehre und Wärmeübertragung, Technische Universität Wien, Wiedner Hauptstrasse 7, A-1040, Wien, Austria
E-mail: kehren@hp.fluid.tuwien.ac.at

Received January 27, 1997

In this paper a new method for the determination of unsteady pressure with a tubing system is shown. The conventional methods try either to optimize the frequency behaviour of the tubing system by implementing restrictors or instantaneous jumps in the cross-sectional area or to correct the measurement by using the transfer function of the tubing system. The new method presented here simply uses a tube with constant, circular cross-section and solves the governing fluid-mechanic equations in the time-domain by numerically propagating in the direction of the spatial axis.

1. INTRODUCTION

To measure time-varying pressures on the surface of models in wind tunnel experiments small pressure transducers with a sufficiently high eigenfrequency are flush-mounted on the modelsurface. If the number of measuring points of one model is too high, one usually uses several tubes which are connected with only one transducer successively during the experiment by a scanivalve. In this paper we consider one of these measuring-tubes. The point of the tube at the model surface is called point A or entrance of the tube; the point of the tube next to the pressure transducer is called point B or end of the tube. The system consisting of the measuring-tube and pressure transducer is called the tubing system.

Berg and Tijdeman [1] derived a method for calculating the transfer function of a tubing system. The transfer function is defined as the ratio of the pressure at the end of the tube over the pressure at the entrance of the tube in the frequency domain. If the maximum frequency of the pressure signal is small enough compared with the acoustic eigenfrequency of the tubing system, which corresponds to the first resonant peak of the transfer function, the pressure at the end and the pressure at the entrance of the tube are nearly identical [2].

0021-9991/98 $25.00

The frequency range of this method is limited due to resonance effects occurring above a certain frequency. To be able to measure signals with higher frequencies restrictors can be implemented inside the tube [8, 5], thus flattening the first resonant peak of the transfer function. Methods to find an effective position of restrictors have been proposed by Gumley [3] and Holmes and Lewis [4]. Sockel and Ottitsch [7] published a paper in which the effect of restrictors was calculated in the time-domain using the method of characteristics in its usual time marching form. Another approach is the correction of the measured signal using the transfer function of the tubing system [5].

In contrast to [7] the direction of the numerical solution procedure is changed in this work. By that way an accurate time-domain method is derived for calculating the pressure at the entrance of a tube from the measured pressure at the end of the tube for high frequencies without the need of restrictors.

In Section 2 the problem and goal of this paper are defined. In Section 3 the assumptions made and the equations governing the problem are given. In Section 4 the numerical solution method is presented and difficulties arising from the type of the stated problem are discussed, especially the problem of stability. In Section 5 comparisons between numerical and experimental results are shown. Finally the characteristics of the scheme are summarized in Section 6.

2. PROBLEM

In Fig. 1 the problem and chosen nomenclature can be seen. Two points A and B are connected by a measuring-tube of length L and constant, circular cross-section with internal diameter d. The bending diameter of the flexible tube-axis is D. At B the tube is ending in a cylindrical cavity with internal volume V. Unsteady pressure p_A in A leads to unsteady pressure p_B in B. The maximum frequency of interest of p_A is f_{max}. Assuming small pressure disturbances the pressure p_A shall be calculated from two given boundary conditions in B, namely the measured pressure p_B and the boundary condition representing the cavity. p_B is given in discretized form with sampling frequency f_s.

In addition to the application described above the method allows us to determine the sum of pressures of several surfacepoints divided by the number of surfacepoints (pneumatic

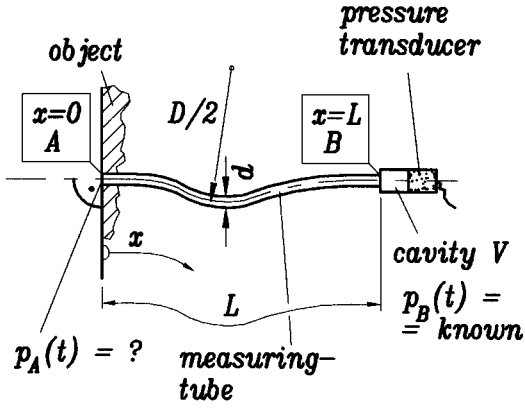

FIG. 1. Problem.

averaging [8]). If each of these points is connected by tubes of the same length and diameter with one manifold, the method presented here yields exactly this result.

3. MATHEMATICAL FORMULATION

The geometrical assumptions concerning the tube are $d/L \ll 1$ and $d/D \ll 1$. The geometrical assumptions regarding the cavity are that the diameter and length of the cavity are of the same order, $V^{1/3}/d \sim O(1)$ and $V^{1/3} f_{max}/a_0 \ll 1$, implying spatially uniform pressure p_B in the cavity. a is the speed of sound. The index 0 indicates the undisturbed state of the fluid. With respect to the fluid-flow we assume an ideal gas, isentropic condition, small pressure disturbances, and axisymmetric, laminar flow. We assume spatially uniform pressure over the tube cross-section. Energy losses at A and B and gravity are neglected. The pressure disturbances are much smaller than the modulus of elasticity of the tube, so d remains constant.

We define the times $t = 0$ and $t = T$ as the beginning and the end of the time interval, during which pressure is measured. The spatial points $x = 0$ and $x = L$ are identified with the entrance A and the end B of the tube (see Fig. 1).

Two different initial-conditions are defined. The zero initial-condition is identical with the fluid being undisturbed for $t = 0$. The undisturbed state is defined by $p = p_0$ and $w = 0$ in the whole tube. w is the mean velocity over the cross-section of the tube. The non-zero initial-condition implies that these values are arbitrary for $t = 0$ and unknown. This is the case if we start our recording at $t = 0$, but we started the experiment earlier, so that waves propagate in the system at $t \le 0$ already.

We define the following dimensionless quantities (1), which are marked by $\tilde{}$,

$$\tilde{x} = \frac{x}{d}, \qquad \tilde{t} = \frac{a_0 t}{d}, \qquad \tilde{f} = \frac{d \cdot f}{a_0}, \qquad \tilde{w} = \frac{w}{a_0}, \qquad \tilde{p} = \frac{p - p_0}{\rho_0 a_0^2}, \qquad \tilde{\tau} = \frac{\tau}{\rho_0 a_0^2}. \quad (1)$$

τ denotes the wall shear stress inside the tube; ρ is the density of the fluid.

Under the assumptions made above the problem can be formulated by using the one-dimensional, linearized continuity (2), the one-dimensional, linearized momentum equation (3), and the linearized boundary condition for the cavity (4),

$$\frac{\partial \tilde{p}}{\partial \tilde{t}} + \frac{\partial \tilde{w}}{\partial \tilde{x}} = 0 \quad (2)$$

$$\frac{\partial \tilde{w}}{\partial \tilde{t}} + \frac{\partial \tilde{p}}{\partial \tilde{x}} + 4\tilde{\tau} = 0 \quad (3)$$

$$\tilde{w}|_{\tilde{x}=L/d} = \frac{4V}{\pi d^3} \frac{d\tilde{p}}{d\tilde{t}}\bigg|_{\tilde{x}=L/d}. \quad (4)$$

$\tilde{\tau}$ is calculated using (5) which is derived in [10] and is valid for laminar, axisymmetric flow,

$$\tilde{\tau}(\tilde{x}, \tilde{t}) = 4\frac{\nu}{a_0 d}\left(2\tilde{w}(\tilde{x}, \tilde{t}) + \int_0^{\tilde{t}} W(\tilde{t} - \tilde{u}) \frac{\partial \tilde{w}(\tilde{x}, \tilde{u})}{\partial \tilde{u}} d\tilde{u}\right). \quad (5)$$

ν is the kinematic viscosity of the fluid. The first term of Eq. (5) is formally identical with the wall shear stress in the case of laminar, steady flow (Hagen–Poiseuille). Therefore the second term of Eq. (5) is usually referred to as the unsteady friction term. It is a memory

integral with weighting function W for past velocity changes. W was derived by Zielke and is given in [10] according to (6),

$$W(s(\tilde{t})) = \begin{cases} 0.282095s^{-0.5} - 1.25 + 1.057855s^{0.5} \\ \quad + 0.9375s + 0.396696s^{1.5} - 0.351563s^2 & \text{for } s < 0.02 \\ \exp(-26.3744s) + \exp(-70.8493s) \\ \quad + \exp(-135.0198s) + \exp(-218.9216s) \\ \quad + \exp(-322.5544s) & \text{for } s > 0.02 \end{cases} \tag{6}$$

with

$$s(\tilde{t}) = 4\frac{\nu}{a_0 d}\tilde{t}. \tag{7}$$

Combining (2) and (3) one obtains the wave equation with a dissipative term. We see that the problem is governed by three nondimensional physical parameters, namely the geometrical parameters $L/d =: \tilde{L}$ and $V/d^3 =: \tilde{V}$ and the friction parameter $\nu/(a_0 d) =: \psi$.

4. NUMERICAL SOLUTION METHOD

The system of equations is solved by applying the method of characteristics. Equations (2) and (3) are transformed onto the characteristic variables $\xi = \tilde{x} - \tilde{t}$ and $\eta = \tilde{x} + \tilde{t}$. Along the characteristic directions (8) and (9), which are straight lines, the compatibility conditions (10) and (11) have to be satisfied,

$$\left.\frac{d\tilde{x}}{d\tilde{t}}\right|_{\xi = const} = +1 \tag{8}$$

$$\left.\frac{d\tilde{x}}{d\tilde{t}}\right|_{\eta = const} = -1 \tag{9}$$

$$\left.\frac{d\tilde{p}}{d\tilde{t}}\right|_{\xi = const} + \left.\frac{d\tilde{w}}{d\tilde{t}}\right|_{\xi = const} = -4\tilde{\tau}|_{\xi = const} \tag{10}$$

$$\left.\frac{d\tilde{p}}{d\tilde{t}}\right|_{\eta = const} - \left.\frac{d\tilde{w}}{d\tilde{t}}\right|_{\eta = const} = +4\tilde{\tau}|_{\eta = const}. \tag{11}$$

Rewriting (8) and (9) as difference equations one obtains

$$\frac{\tilde{\Delta}x}{\tilde{\Delta}t} = 1, \tag{12}$$

where $\tilde{\Delta}x$ and $\tilde{\Delta}t$ stand for the distance of grid points in the $\tilde{x}$- and $\tilde{t}$-direction. The Courant number of the scheme is 1, therefore the shift condition is met exactly, which guarantees maximum accuracy.

By the discretization a nondimensional numerical parameter is introduced, namely $\tilde{\Delta}t$. For practical reasons Δt is chosen to be constant and equal the reciprocal of the sampling frequency of the measured signal $\Delta t = 1/f_s$ and therefore $\Delta\tilde{t} = 1/\tilde{f}_s$.

The derivative in (4) is discretized by its first order backward difference expression. Equation (5) is discretized as

$$\tilde{\tau}(\tilde{x}_i, \tilde{t}_j) = 4\psi\left(2\tilde{w}(\tilde{x}_i, \tilde{t}_j) + \sum_{k=1}^{\mathsf{kend}} \mathsf{Winte}_k \cdot \mathsf{dwdt}_k\right) \tag{13}$$

with

$$\mathsf{Winte}_k = \int_{(k-1)\Delta\tilde{t}}^{k\Delta\tilde{t}} W(\tilde{t})\, d\tilde{t}, \qquad k = 1, 2, \ldots \tag{14}$$

and

$$\mathsf{dwdt}_k = (\tilde{w}(\tilde{x}_i, \tilde{t}_j - (k-1)\Delta\tilde{t}) - \tilde{w}(\tilde{x}_i, \tilde{t}_j - k\Delta\tilde{t}))/\Delta\tilde{t}, \qquad k = 1, 2, \ldots. \tag{15}$$

For the problems discussed here kend can be chosen as $\mathsf{kend} \approx 30$.

The calculation is done under the assumption of the zero initial-condition. This is a purely numerical assumption. We emphasize that this numerical initial-condition need not be identical with the physical initial-condition, which in most practical cases will be an unknown non-zero initial-condition. We will show later that the dependence of the solution on the physical initial-condition decreases with time rather rapidly, if friction effects are high enough. This is the case for usual measuring-tubes. Therefore a physical non-zero initial-condition will pose no problem for our scheme.

4.1. *Time Marching Algorithm*

For a better understanding we first briefly explain the algorithm in its conventional form, which is a time marching algorithm, although this does not work for our problem.

For "usual" hyperbolic problems the number of physical boundary conditions at each boundary is equal to the number of characteristics pointing into the region, as time increases. Thus the problem is well-posed [9]. In our case this would be one physical boundary condition at A and one at B.

The principle of time marching in the $\tilde{x} - \tilde{t}$-plane using the method of characteristics is shown in Fig. 2. The flowfield is calculated in an explicit way by propagating numerically

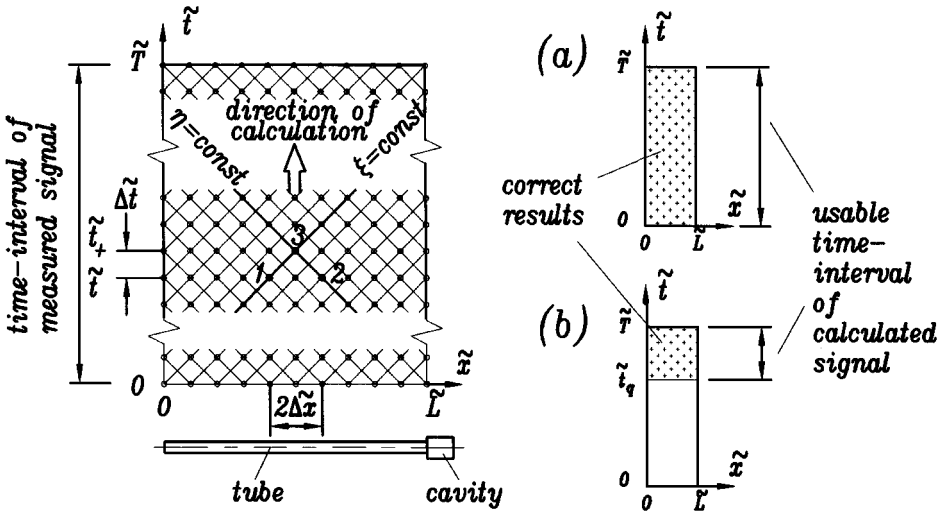

FIG. 2. Principle of time marching in the $\tilde{x} - \tilde{t}$-plane; regions containing correct results for (a) physical zero initial-condition and (b) unknown physical non-zero initial-condition.

in the direction of the time axis. The compatibility equations (10) and (11) can be written as difference equations (16) and (17), where the indices correspond to those shown in Fig. 2,

$$\tilde{p}_3 - \tilde{p}_1 + \tilde{w}_3 - \tilde{w}_1 = -4\tilde{\Delta}t \cdot \tilde{\tau}_1 \tag{16}$$

$$\tilde{p}_3 - \tilde{p}_2 - \tilde{w}_3 + \tilde{w}_2 = +4\tilde{\Delta}t \cdot \tilde{\tau}_2. \tag{17}$$

With Eqs. (16) and (17), $\tilde{p}$ and $\tilde{w}$ inside the duct are calculated. The physical boundary conditions together with the compatibility conditions (17) and (16) are used for the determination of the unknown $\tilde{p}$ and $\tilde{u}$ at A and B, respectively.

Neglecting the memory integral in (5), $\tilde{\tau}$ diminishes all dynamic disturbances, i.e., disturbances with $\tilde{f} > 0$, exponentially. We define a critical frequency $\tilde{f}_{crit}$,

$$\tilde{f}_{crit} = \frac{16\psi}{2\pi}. \tag{18}$$

Frequencies higher than $\tilde{f}_{crit}$ are damped with $\exp(-16\psi\tilde{t})$ as time increases. The time $\tilde{t}_q$ after which such a disturbance has decreased to less than q times its initial amount can be estimated,

$$\tilde{t}_q = \frac{\ln(q^{-1})}{16\psi}. \tag{19}$$

For the cases discussed here the critical frequency $\tilde{f}_{crit}$ is smaller than the maximum frequency of interest $\tilde{f}_{max}$. Therefore it makes sense to use (19) for an estimation of the time $\tilde{t}_q$ of influence of disturbances, e.g., introduced by a discrepancy between the numerical and physical initial-condition. $q = 0.01$ is appropriate to estimate $\tilde{t}_q$.

On the right-hand side of Fig. 2 the regions in the $\tilde{x} - \tilde{t}$-plane containing correct results for the two cases of (a) a physical zero initial-condition and (b) an unknown physical non-zero initial-condition are shown. For usual tubing systems $\tilde{t}_q$ is sufficiently small.

4.2. *Space Marching Algorithm*

For the problem discussed here the time marching algorithm does not work, since we have two boundary conditions at B, namely measured pressure p_B and Eq. (4), and none at A.

The problem is solved by changing the direction of integration. The flowfield is calculated by propagating numerically in the direction of the spatial axis. The principle of space marching in the $\tilde{x} - \tilde{t}$-plane using the method of characteristics is shown in Fig. 3.

The compatibility equations (10) and (11) can be written as difference equations (20) and (21), where the indices correspond to those shown in Fig. 3,

$$\tilde{p}_1 - \tilde{p}_3 + \tilde{w}_1 - \tilde{w}_3 = -4\tilde{\Delta}t \cdot \tilde{\tau}_1 \tag{20}$$

$$\tilde{p}_3 - \tilde{p}_2 - \tilde{w}_3 + \tilde{w}_2 = +4\tilde{\Delta}t \cdot \tilde{\tau}_2. \tag{21}$$

The numerical procedure starts with the calculation of $\tilde{w}_B$ from $\tilde{p}_B$ using (4) and of $\tilde{\tau}_B$ using (5). After that the following two steps, defining an explicit scheme, are repeated until A is reached: First $\tilde{p}$ and $\tilde{w}$ at $\tilde{x}_- = \tilde{x} - \tilde{\Delta}x$ are calculated using (20) and (21). Secondly $\tilde{\tau}$ at the new spatial coordinate is determined using (5).

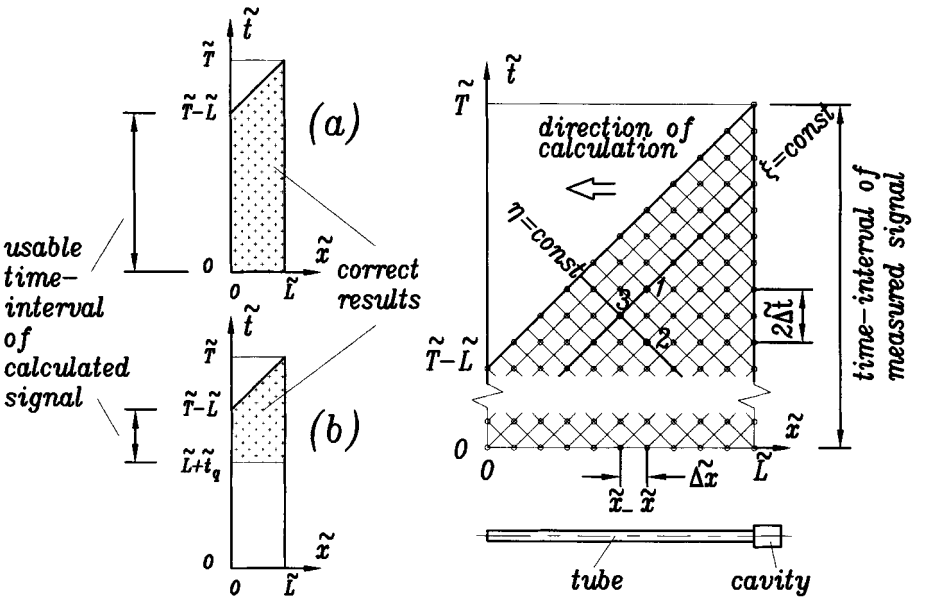

FIG. 3. Principle of space marching in the $\tilde{x}-\tilde{t}$-plane; regions containing correct results for (a) physical zero initial-condition and (b) unknown physical non-zero initial-condition.

It is obvious that the field of the calculated values is limited by the characteristic line $\xi = \text{const}$ through point $(\tilde{L}, \tilde{T})$. Therefore the signal at A can be calculated only for times within the interval $[0, \tilde{T} - \tilde{L}]$. By choosing $\tilde{T}$ large enough this fact poses no problem.

As indicated above, on the axis $\tilde{t} = 0$ the numerical initial-condition is the zero initial-condition, without taking into account the physical initial-condition. In the case of a physical non-zero initial-condition the scheme therefore produces wrong results at all points $(\tilde{x}, \tilde{t})$ under the characteristic line $\eta = \text{const}$ through point $(\tilde{L}, 0)$. With no friction present the scheme gives the correct result for $\tilde{p}_A$ for times in the interval $[\tilde{L}, \tilde{T} - \tilde{L}]$, since in this case the above mentioned points in the $\tilde{x} - \tilde{t}$-plane are not needed at all. Mathematically speaking the calculation of $\tilde{p}_A$ in the time-interval $[\tilde{L}, \tilde{T} - \tilde{L}]$ with no friction present is a well-posed problem, since this interval lies in the region of determination. In the case of friction present (and of course in the case of a physical non-zero initial-condition) $\tilde{\tau}$ obviously gets wrong for all points under and near the characteristic line $\eta = \text{const}$ through point $(\tilde{L}, 0)$. However, due to the friction this error decreases exponentially with time (19) and therefore is of negligible effect for times $\tilde{t} > \tilde{L} + \tilde{t}_q$. Therefore the problem of calculating p_A in the time-interval $[\tilde{L} + \tilde{t}_q, \tilde{T} - \tilde{L}]$ with friction present is also well posed.

On the left-hand side of Fig. 3 the regions in the $\tilde{x} - \tilde{t}$-plane containing correct results for the two cases of (a) a physical zero initial-condition and (b) an unknown physical non-zero initial-condition are shown.

Now we come to the fundamental difference between time and space marching, which is responsible for the main difficulty of the space marching method. The difference comes from the friction term in (3).

A Von Neumann stability analysis shows that the space marching algorithm as presented up to now is unstable. Physically speaking this instability is due to the fact that we are calculating "against" $\tilde{\tau}$ on the characteristic lines $\xi = \text{const}$. In Fig. 3 one can easily see that the information from point 1 is needed to calculate $\tilde{p}_3$ and $\tilde{w}_3$. Therefore artificial viscosity

is added to stabilize the solution, which was done by replacing $\tilde{p}$ and $\tilde{w}$ by $\tilde{p}_d$ and $\tilde{w}_d$ according to (22) after each spatial step,

$$\begin{aligned}\tilde{p}_d(\tilde{x},\tilde{t}) &= \tilde{p}(\tilde{x},\tilde{t}) + b\cdot[\tilde{p}(\tilde{x},\tilde{t}-\tilde{\Delta}t) - 2\cdot\tilde{p}(\tilde{x},\tilde{t}) + \tilde{p}(\tilde{x},\tilde{t}+\tilde{\Delta}t)]\\ \tilde{w}_d(\tilde{x},\tilde{t}) &= \tilde{w}(\tilde{x},\tilde{t}) + b\cdot[\tilde{w}(\tilde{x},\tilde{t}-\tilde{\Delta}t) - 2\cdot\tilde{w}(\tilde{x},\tilde{t}) + \tilde{w}(\tilde{x},\tilde{t}+\tilde{\Delta}t)].\end{aligned} \tag{22}$$

A Von Neumann stability analysis for the scheme with artificial viscosity (22), neglecting the memory integral in (5), shows that the scheme becomes stable, if b is chosen according to

$$\begin{aligned} b \in \left[b_{min}, \frac{1}{2}\right], \qquad b_{min} &= \frac{1}{2}\left(1 - \frac{1}{16\psi\tilde{\Delta}t + \sqrt{1+(16\psi\tilde{\Delta}t)^2}}\right)\\ &= 8\psi\tilde{\Delta}t + O((\psi\tilde{\Delta}t)^2).\end{aligned} \tag{23}$$

By implementing artificial viscosity (22) the amplification matrix of the numerically undamped scheme is multiplied by the term in square brackets of

$$\begin{gathered}\left[1 - 2b\left(1 - \cos\left(2\pi\frac{\tilde{f}_n}{\tilde{f}_s}\right)\right)\right]^{\tilde{L}\cdot\tilde{f}_s} = 1 - q_n; \qquad \tilde{f}_s = \tfrac{1}{\tilde{\Delta}t},\ \tilde{f}_n = \tfrac{n}{2\tilde{T}},\\ n = 0, 1, \ldots, \tilde{T}\cdot\tilde{f}_s.\end{gathered} \tag{24}$$

$\tilde{f}_s$ is the dimensionless sampling frequency. The exponent $\tilde{L}\cdot\tilde{f}_s$ of the term in square brackets of (24) is equal to the number of $\tilde{\Delta}x$-steps necessary to cover the length of the tube. The frequencies $\tilde{f}_n$ are the numerically relevant frequencies determined by the grid spacing. At each $\tilde{\Delta}x$-step the amplitude corresponding to a frequency $\tilde{f}_n$ is multiplied by the term in square brackets of (24). This multiplication factor acts like a low pass filter, which has no effect when $n = 0$ and a maximum effect when $n = \tilde{T}\cdot\tilde{f}_s$. The scheme can be stabilized but becomes less accurate at the same time. q_n is the relative error introduced by (22) on the frequency $\tilde{f}_n$. b should be chosen as $b \le 0.25$. Otherwise the multiplication factor becomes negative at higher frequencies, which indicates that the high frequency behaviour of (22) does not make sense any more.

Due to the low pass filter effect of (22) the sampling frequency $\tilde{f}_s$ has to be chosen large enough compared to the maximum frequency of interest $\tilde{f}_{max}$. To estimate the necessary sampling frequency $\tilde{f}_s$ we use (24) with b replaced by $8\psi/\tilde{f}_s \approx b_{min}$ according to (23) and $\tilde{f}_n$ replaced by the maximum frequency of interest $\tilde{f}_{max}$. Then the quadratic approximation of (24) for $1/\tilde{f}_s \to 0$ is

$$\left(\frac{\tilde{f}_s}{\tilde{f}_{max}}\right)^2 = \frac{32\pi^2\psi\tilde{L}}{q_{max}}. \tag{25}$$

For given $\tilde{f}_{max}$, ψ, and $\tilde{L}$ and chosen q_{max}, which should be $q_{max} \approx 0.1$, $\tilde{f}_s$ can be estimated using (25). With $\tilde{f}_s$ one can calculate b_{min} using (23). We propose to choose $b \approx 10\cdot b_{min}$. With $\tilde{f}_s$ and b the error q_n introduced by (22) on a frequency $\tilde{f}_n$ can be calculated with (24).

5. VERIFICATION OF THE METHOD

The quality of the method is shown in the following three subsections. First an experimental verification demonstrates that the method works well with long and short tubes, that

the memory integral is of importance, and that a physical non-zero initial-condition is no serious problem. In the second subsection we show that the scheme converges to the correct solution, as the stepsizes are refined. Finally we compare the scheme with the method of Irwin, Cooper, and Girard [5], who first measured the transfer function experimentally and then performed a numerical correction of measured pressure in the frequency domain.

All subsequent measurements were done with air under atmospheric conditions, $p_0 = 100$ kPa, $\rho_0 = 1.19$ kg/m^3, $a_0 = 343$ m/s, and $\nu = 15.3 \cdot 10^{-6}$ m^2/s. In all figures of this section relative pressure histories with respect to the ambient pressure p_0 are shown.

5.1. *Experimental Verification*

The experimental setup consists of a pressure wave generator, a primary tube, the measuring tube, and two pressure transducers. The pressure wave generator, which is described in [6], produces a plane pressure wave, which propagates along the primary tube. The measuring tube is connected with the primary tube in point A. One pressure transducer is positioned in the same cross-section of the primary tube as point A to measure p_A. The second pressure transducer is positioned at the end of the measuring tube to measure p_B.

d and V have to be determined accurately once for a certain tube-cavity configuration by one calibration measurement, at which p_A and p_B are measured. By several calibration measurements we found out that d and V do not change at all for one configuration later on.

In each of the Figs. 4 to 7 three curves are shown, namely p_A calculated with the new solution procedure, measured pressure p_A, and measured pressure p_B, which is the input for the calculation. By comparing the calculated and measured pressure p_A one can see the quality of the method.

For all results shown in this subsection there was $V = 280$ mm^3. $b = 0.1$ was chosen in the stability region of the scheme (23) (ψ and $\tilde{\Delta}t$ are given in the next two paragraphs). The signals with a maximum frequency of interest $f_{max} \approx 350$ Hz were sampled with $f_s = 20$ kHz. This results in a value of 0.99879 for the term in square brackets of (24).

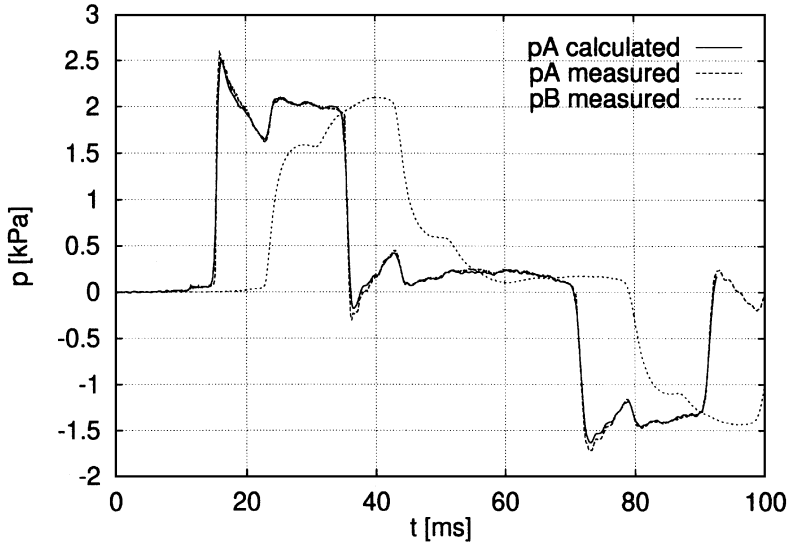

FIG. 4. Calculation and measurement: plastic tube, $d = 1.20$ mm, $L = 2.50$ m, $V = 280$ mm^3, $f_s = 20$ kHz; with memory integral; physical zero initial-condition.

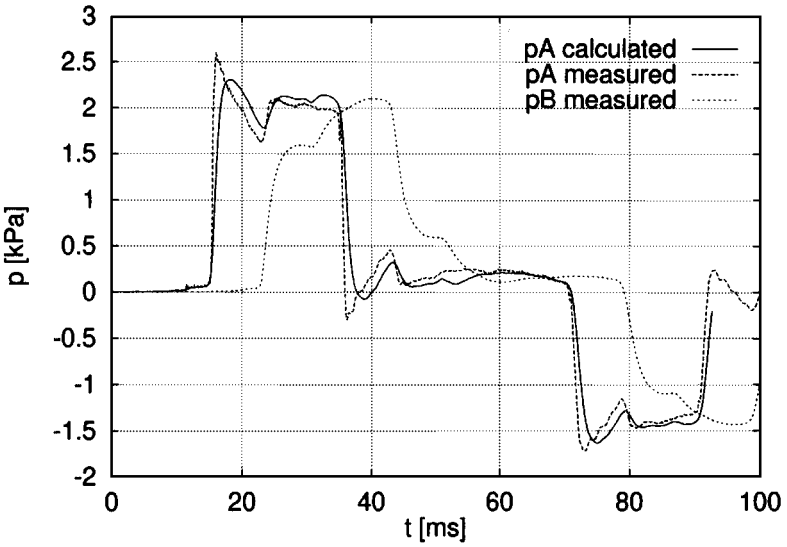

FIG. 5. Calculation and measurement: plastic tube, $d = 1.20$ mm, $L = 2.50$ m, $V = 280$ mm^3, $f_s = 20$ kHz; without memory integral; physical zero initial-condition.

In Fig. 4 the calculation for a plastic tube with flexible axis, $L = 2.50$ m and $d = 1.20$ mm can be seen. The corresponding nondimensional parameters are $\tilde{L} = 2083$, $\tilde{V} = 162$, $\psi = 3.72 \cdot 10^{-5}$, and $\tilde{\Delta}t = 14.3$. q_{max} according to (24) with $f_n = f_{max} = 350$ Hz amounts to $q_{max} = 16.14\%$. The average error is of the order of 1%. No influence of D could be detected for $D/d \approx 20$. In Fig. 5 the result achieved with the data of the same measurement but neglecting the memory integral term in (5) can be seen. The average error is of the order of 10%. Comparing Figs. 4 and 5 one can easily see the importance of the memory integral

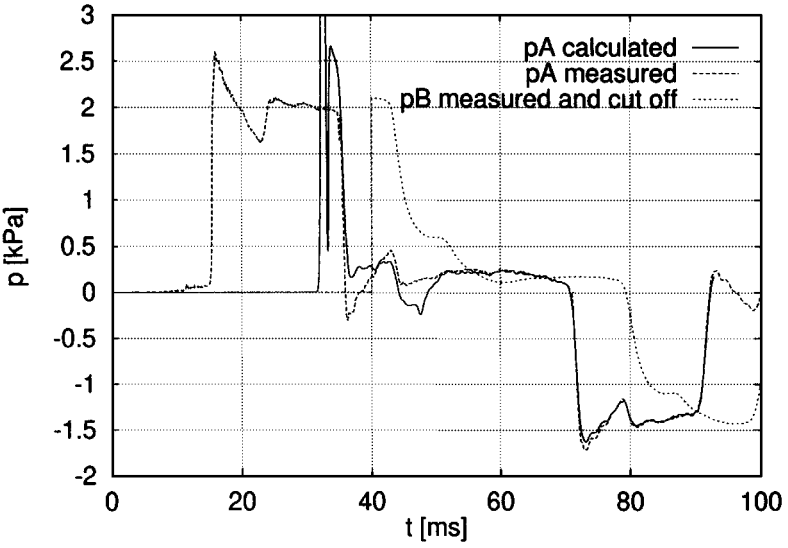

FIG. 6. Calculation and measurement: plastic tube, $d = 1.20$ mm, $L = 2.50$ m, $V = 280$ mm^3, $f_s = 20$ kHz; with memory integral; p_B cut off at $t = 40$ ms.

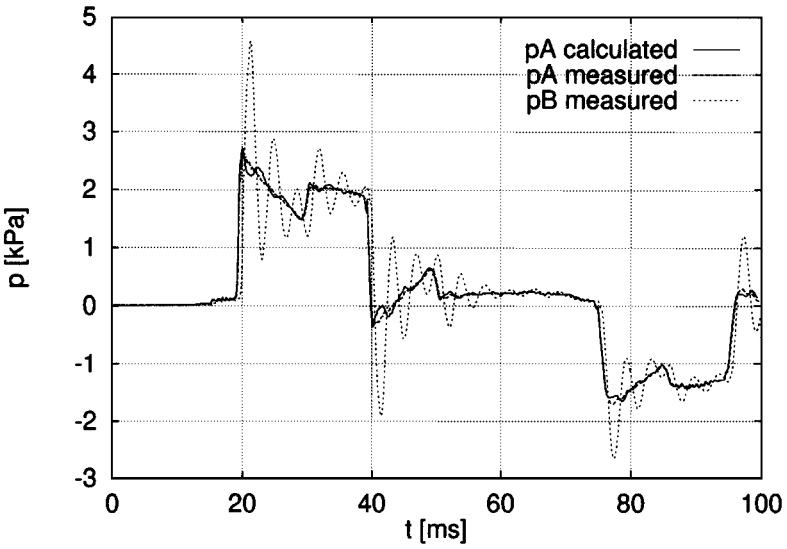

FIG. 7. Calculation and measurement: aluminum tube, $d = 1.60$ mm, $L = 0.19$ m, $V = 280$ mm^3, $f_s = 20$ kHz; with memory integral; physical zero initial-condition.

term in (5). Neglecting this term produces a scheme with little accuracy at high frequencies. In Fig. 6 the signal p_B is cut off at $t = 40$ ms, which introduces a disturbance. Comparing Figs. 4 and 6 one can see that the error introduced by the initial jump of the data has no influence on p_A after $t \approx 50$ ms. Therefore $t_{q,effective} \approx 3\,\text{ms} < t_q = 27$ ms from (19) with $q = 0.01$ and (1).

In Fig. 7 the calculation done for an aluminum tube with $L = 0.19$ m and $d = 1.60$ mm is shown. The corresponding nondimensional parameters are $\tilde{L} = 119$, $\tilde{V} = 68$, $\psi = 2.79 \cdot 10^{-5}$, and $\tilde{\Delta}t = 10.7$. This results in $q_{max} = 1.34\%$ according to (24) with $f_n = f_{max} = 350$ Hz. The dominant frequency of p_B is the acoustic eigenfrequency of the system. The new solution procedure works properly with such signals.

5.2. *Numerical Convergence*

Here it is shown that the difference between the numerical and correct solution tends to zero as the stepsizes are refined. For this purpose the measurement from the above subsection with the plastic tube with $L = 2.50$ m, $d = 1.20$ mm, and $f_s = 20$ kHz is taken. Using only every twentieth, tenth, and fourth point of p_B results in smaller frequencies $f_s = 1$ kHz, $f_s = 2$ kHz, $f_s = 5$ kHz and larger timesteps. Performing calculations with these data results in the curves shown in Fig. 8. The sampling frequencies $f_s = 1$ kHz and $f_s = 2$ kHz are definitely too small and lead to an unsatisfactory behaviour at high frequencies. The result with $f_s = 5$ kHz is good. The scheme converges to the correct solution as the stepsizes tend to zero.

5.3. *Comparison with the Method of Irwin, Cooper, and Girard*

Finally our method is compared with the method proposed by Irwin, Cooper, and Girard [5]. Using this method [5] one measures the transfer function of the tubing system experimentally and corrects the measured pressure p_B numerically in the frequency domain using the measured transfer function.

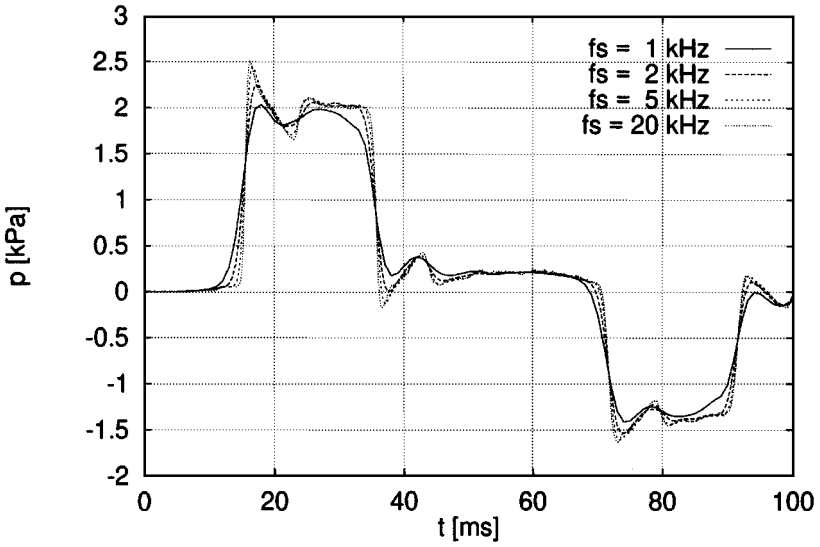

FIG. 8. Convergence of the solution as stepsizes are refined $f_s \to \infty$.

Our calculation is done using the measurement with the PVC tube with $L = 10\,\text{ft} = 3.05\,\text{m}$ taken from [5, Fig. 6]. The pressure scale is not specified, which poses no problem, since the problem is linear. Volume and diameter are given in [5] to be $V = 80\,\text{mm}^3$ and $d = 1.35\,\text{mm}$. It turned out that the diameter must be chosen $d = 1.15\,\text{mm}$ for our method to give a good result. This is due to the fact that the roughness of the PVC tube results in an effective inner diameter which is smaller than the macroscopically visible and measured diameter. That is why a calibration measurement is necessary when our method is used (see above).

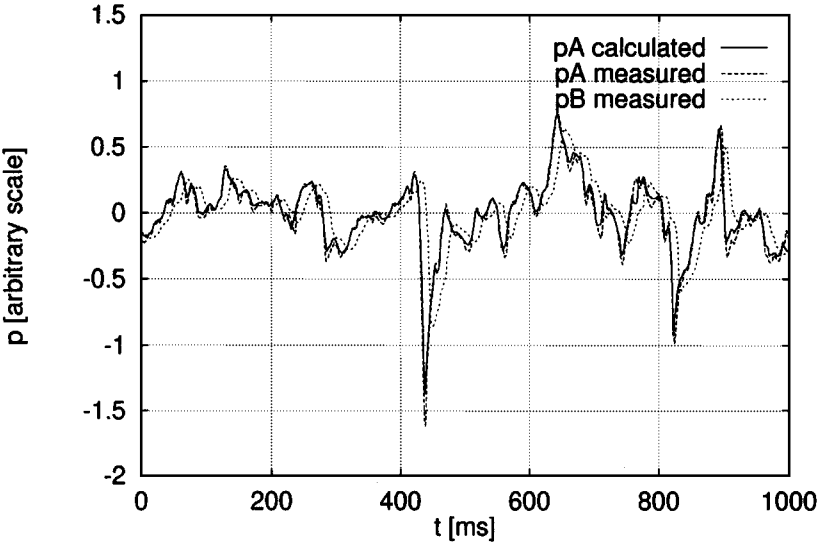

FIG. 9. Calculation done with data of Irwin, Cooper, and Girard. PVC tube, $d = 1.15$ mm, $L = 3.05$ m, $V = 80\,\text{mm}^3$, $f_s = 1$ kHz.

p_A calculated and measured and p_B measured are shown in Fig. 9. The result is of approximately the same quality as in [5] with the exception of the peak at $t = 437$ ms. This is most probably due to the fact that we had to get the data directly out of the figure, which certainly caused a loss of information.

6. CONCLUSION

The new solution procedure presented here is a useful tool for calculating the pressure p_A at the entrance of a tube from the measured pressure p_B at the end of the tube directly in the time-domain. The average error of the scheme is of the order of 1%. The measuring tube has constant circular cross-section without restrictors. The tube can be very long. High frequencies pose no problem, if the sampling frequency is large enough. The method also works correctly, if the fluid is not at rest at the beginning of the measurement, provided that friction effects are high enough. The geometrical parameters have to be determined by one calibration measurement.

REFERENCES

1. H. Berg and H. Tijdeman, *Theoretical and Experimental Results for the Dynamic Response of Pressure Measuring Systems*, Tech. Rep. NLR-TRF 238, National Aero and Aeronautical Research Institute, 1965.
2. N. J. Cook, Adapting the DISA 51F32 low pressure transducer for use in pressure scanning switches, *J. Phys. E* **8**, 267 (1975).
3. S. J. Gumley, A detailed design method for pneumatic tubing systems, *J. Wind Eng. Ind. Aerodyn.* **13**, 441 (1983).
4. J. D. Holmes and R. E. Lewis, Optimization of dynamic-pressure-measurement systems, *J. Wind Eng. Ind. Aerodyn.* **25**, 249 (1987).
5. H. P. A. H. Irwin, K. R. Cooper, and R. Girard, Correction of distortion effects caused by tubing systems in measurements of fluctuating pressures, *J. Ind. Aerodyn.* **5**, 93 (1979).
6. F. Ottitsch, *Schwache mehrdimensionale Druckwellen in Rohrleitungen zufolge unstetiger Querschnittsänderungen am Beispiel der Eisenbahnaerodynamik*, Ph.D. thesis, Technical University, Vienna, 1995.
7. H. Sockel and F. Ottitsch, Numerical and experimental investigation of a pressure measuring system with a restrictor, *J. Wind Eng. Ind. Aerodyn.* **42**, 975 (1992).
8. T. Statopoulos, *Technique of Pneumatically Averaging Pressure*, Tech. Rep. BLWT-Report-2-75, The University of Western Ontario, 1975.
9. G. B. Whitham, *Linear and Nonlinear Waves* (Wiley, New York, 1974).
10. W. Zielke, Frequency-dependent friction in transient pipe flow, *J. Basic Engrg.* **90**, 109 (1968).